CHAPTER III

RESULTS

Two animals died during anesthesia in study III and were not replaced. All the animals had normal behavior after surgery and can applied full weight to their hind limbs within one day after the operation and remained in excellent health throughout the course of the experiment. The surgical site healed normally and no adverse reactions or signs of infection were observed. When dissecting and removing the tissue above the chambers, no sign of inflammation or other adverse reactions could be observed except in two animals in study III which had presumptive infection on one of their surgical sites at the time of sacrifice and the results obtained from these two defects were dropped from the analyses. Some dense connective tissue scarring could be found surrounding the chambers in some animals.

Study I

Quantitation of bone regeneration

The histomorphometric results of bone regeneration in cortical and supracortical defect appear in **Table 3**. The specimens harvested from day 3 revealed loose connective tissue and mesenchymal cells with small blood vessels in cortical defect area. Supracortical area was filled with blood clot formation and packed red blood cells. No bone trabeculae were detected in either the cortical defect or supracortical area but mild infiltration of inflammatory cells was noticed in the

Table 3 Area of new bone regeneration at given time point expressed as % of the total defect area (mean ± SD)

	Day 3	Day 7	Day 21	Day 28
% bone in the cortical defect area	0	40.32 ± 4.98	40.40 ± 10.14	59.59 ± 7.31
% bone in the supracortical area	0	12.31 ± 1.24	44.37 ± 5.57	56.35 ± 15.03

connective tissue at cortical defect area (**Figure 4A**). At day 7, histological sections revealed immature new bone trabeculae which were embedded in a fibrovascular stroma in the cortical defect area (**Figure 4B**). The amount of bone ingrowth (percent of new bone within the defect area) was 40.32 ± 4.98% (mean ± SD) with a range of 35-47%. Dense connective tissue was found in almost all the supracortical area with some immature new bone trabeculae close to the cortical defect area. The amount of new bone in the supracortical area was 12.31 ± 1.24% with the range of 10-15%. The specimens harvested from day 21 contained more mature and thicker trabecular bone compared to trabecular bone found in day 7 both in the cortical defect and supracortical area (**Figure 4C**). The amount of bone ingrowth in the cortical defect area was 40.40 ± 10.14% with a range of 28-51%. The amount of bone ingrowth in the supracortical area was 44.37 ± 5.57% with a range of 36-49%. At day 28, more bone was found in both in the cortical defect area and the supracortical area with an area of 59.59 ± 7.31% (range 52-72%) and 56.35 ± 15.03%(range 39-66%)

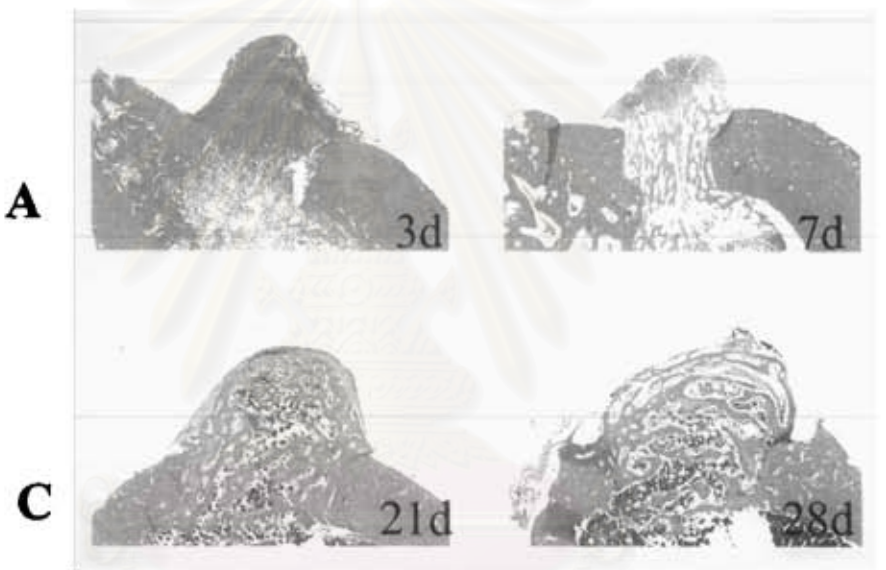

Figure 4 Photomicrograph demonstrating bone regeneration in the cortical defect and supracortical area. (A) 3 days, (B) 7 days, (C) 21 days and (D) 28 days after surgery (original magnification x20)

respectively. In addition, bone ingrowth in the defect revealed more mature and cortical-bone like (**Figure 4D**).

Localization of mitotic activity

At day 3, incorporation of BrdU was found mainly at the cortical defect area with dispersely distribute pattern. In day 7, BrdU labeled cells were found predominantly in the supracortical area directly beneath the titanium chamber which occupied more than half of the supracortical area. Some area at the center of bone marrow space also had BrdU positive cells. Positive mitotic cells were found in the marrow space in the sections from day 21 but a fewer number of positive cells were found at the supracortical area beneath the titanium chamber compared to day 7. At day 28, BrdU incorporated cells were found at the appositional growth site on periosteal surface in additional to the area in bone marrow and the supracortical area.

COX-2 Expression

The time-dependent expression of COX-2 is shown in **Figure 7**. Maximal COX-2 was observed at day 3 ($3.16 \pm 0.44\%$ of total area). It quickly subsided by 7 days and persisted at low levels through day 28 (1.05 ± 0.17). The early expression of COX-2 at day 3 is shown in **Figure 5A** demonstrating the localization of COX-2 in condensed mesenchymal cells which are replacing the blood clot especially in juxtaposition with the condensed mesenchymal tissue and packed red blood cells or blood clot. At day 7, the small amount of COX-2 expression was found in the same area and also in the cells in the newly formed bone trabeculae. Some bone lining cells and osteocytes also expressed COX-2 at day 21 and 28.

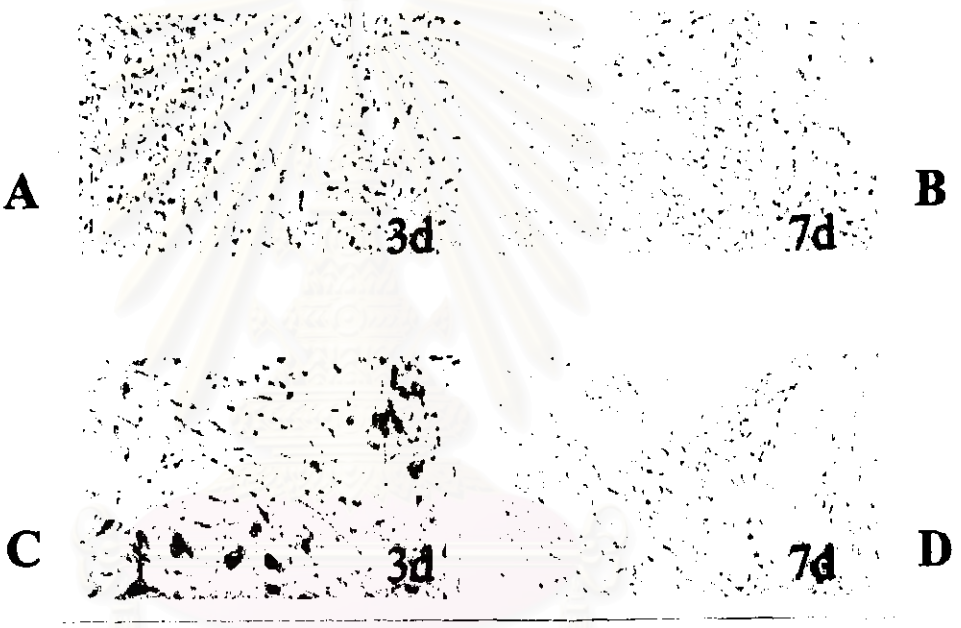

Figure 5 Photomicrograph demonstrating immunohistochemistry staining of COX-2 (A and B), PDGF-B (C and D) at 3 days (A and C), and 7 days (B and D) (original magnification x200)

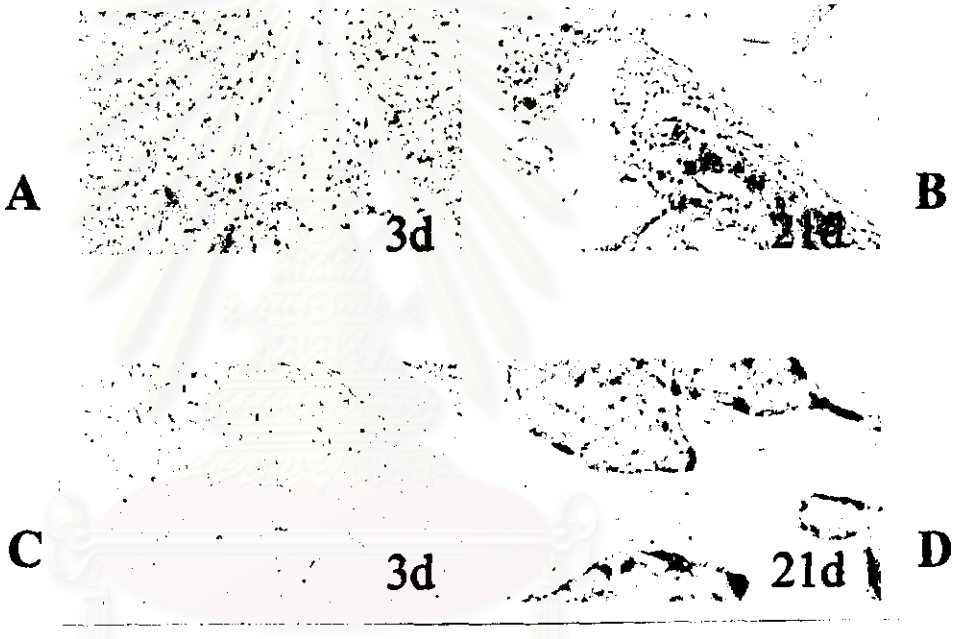

Figure 6 Photomicrograph demonstrating immunohistochemistry staining of BMP-6 (A and B), IGF (C and D) at 3 days (A and C) and 21 days (B and D) (original magnification x200)

PDGF-B Expression

As with COX-2, PDGF-B expression peaks at day 3 (2.55 ± 0.46) and decreases dramatically by day 7 (0.14 ± 0.07) and remains low through day 28 (0.04 ± 0.02). PDGF-B is localized markedly in mesenchymal cells in dense connective tissue in day 3. Some positive cells are found in blood clot area. Very weak staining and very few positive cells are found at day 7 through day 20 (**Figure 5B and 8**).

BMP-6 Expression

The expression of BMP-6 is shown in **Figure 6A and 9**. Maximal BMP-6 expression is evident at day 3 (7.05 ± 1.60) and slowly decreases through days 7 (5.99 ± 1.19), 21 (5.07 ± 0.83) and 28 (3.08 ± 0.43). In contrast to the early rise and fall of COX-2 and PDGF-B, the signal for BMP-6 decreases slightly, but remains evident throughout day 28. BMP-6 expression at day 3 appears in newly formed dense connective tissue as well as in blood clot. At day 7, BMP-6 positive cells were found in connective tissue between bone trabeculae and in extra cellular matrix surrounded the cells. Osteocytes also expressed different degree of BMP-6 expression which decreased in day 28. In day 21 samples, some osteoblasts and bone lining cells were positively stained. Interestingly, some osteoclasts and the bone surface beneath the osteoclasts also expressed BMP-6. A small number of bone lining cells and osteocytes were positively stained at day 28.

IGF Expression

IGF expression increases monotonically from day 3 (2.01 ± 0.58) to reach a maximum by day 28 (6.68 ± 0.68). The distribution of IGF appears localized in both condense mesenchymal tissue and in blood clot area in day 3. Increased expression

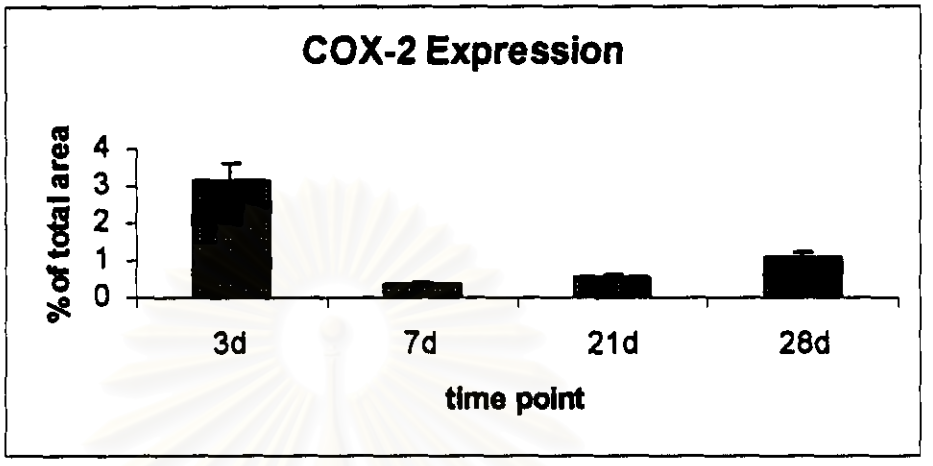

Figure 7 Expression of COX-2 during different time point of bone regeneration

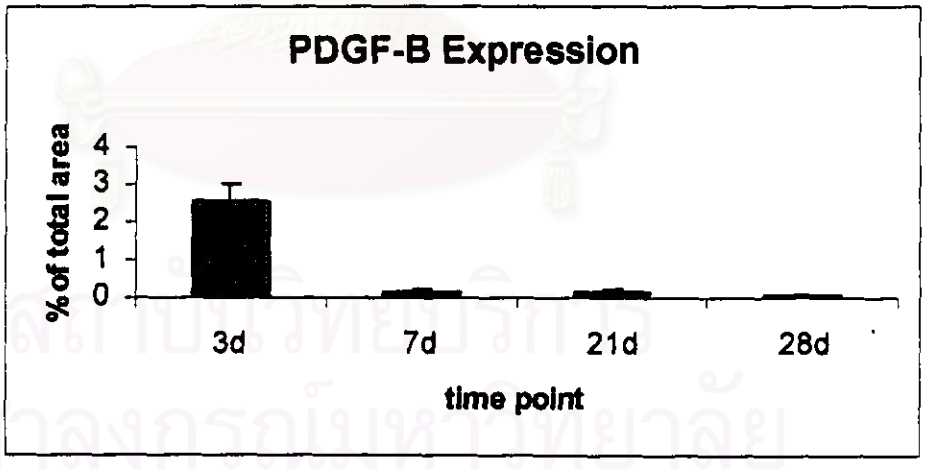

Figure 8 Expression of PDGF-B during different time point of bone regeneration

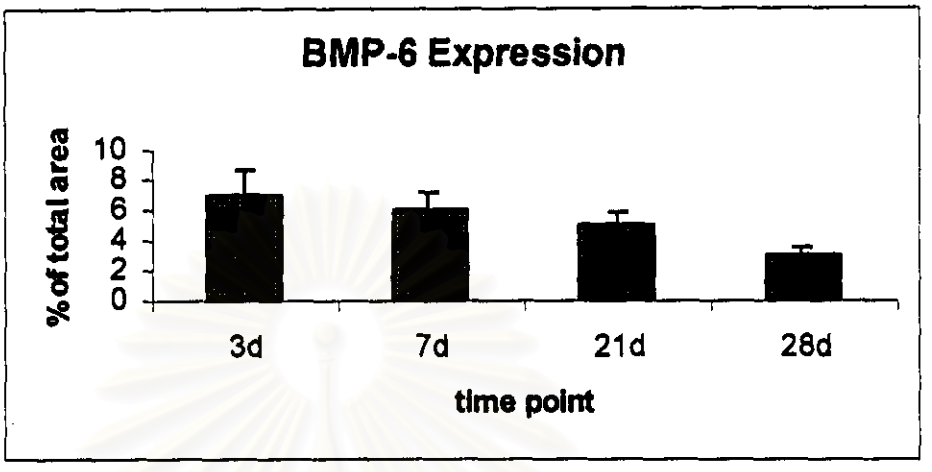

Figure 9 Expression of BMP-6 during different time point of bone regeneration

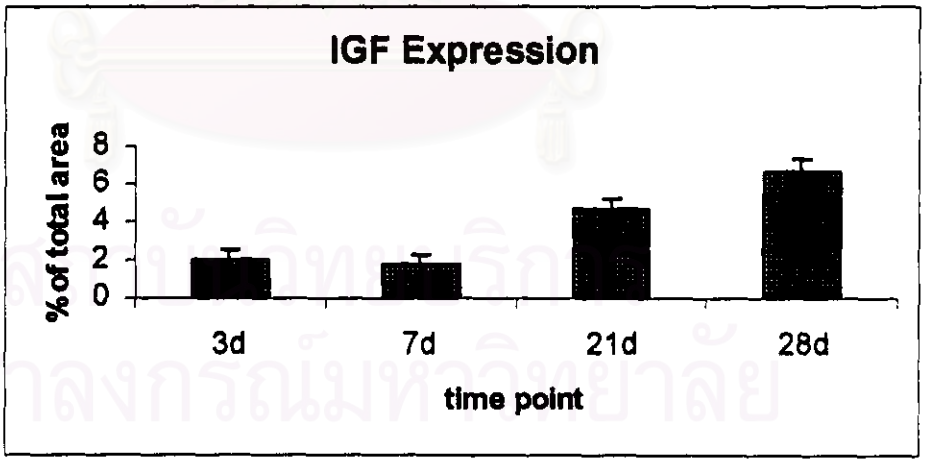

Figure 10 Expression of IGF during different time point of bone regeneration

was found in osteocytes in day 7 and in osteoblasts and cuboidal bone lining cells both in day 21 and 28 (**Figure 6B and 10**).

Study II

The effect of COX-2 inhibitor (NS-398) on area of new bone regeneration in cortical and supracortical defect was shown in **Figure 12**. In animals injected with NS-398, a decrease in bone area in both the cortical and supracortical defect region were noticed with significantly decrease of about 25% in supracortical defect (**Figure 11**). Moreover, less mature new bone was found in animals treated with NS-398 (**Figure 12B and 12D**) compared to those of the control (**Figure 12A and 12C**). By using immunohistochemistry, NS-398 treatment demonstrated that decreasing of COX-2, BMP-6 and PDGF-B expression in cortical defect (**Figure 13**) with significant difference in COX-2 and BMP-6 expression (decreased 60% and 50% respectively). NS-398 significantly increased IGF expression about 150% in cortical defect area. By using RT-PCR, a significant decrease in mRNA level of BMP-2, BMP-6 (decreased 41% and 65% respectively). could be detected in supracortical part, whereas PDGF-A and PDGF-B mRNA expression remained unchanged in supracortical defect (**Figure 14 and 15**). In cortical defect area, no significant different in mRNA level was seen except PDGF-A. NS-398 significantly increased PDGF-A mRNA in cortical defect (**Figure 15**).

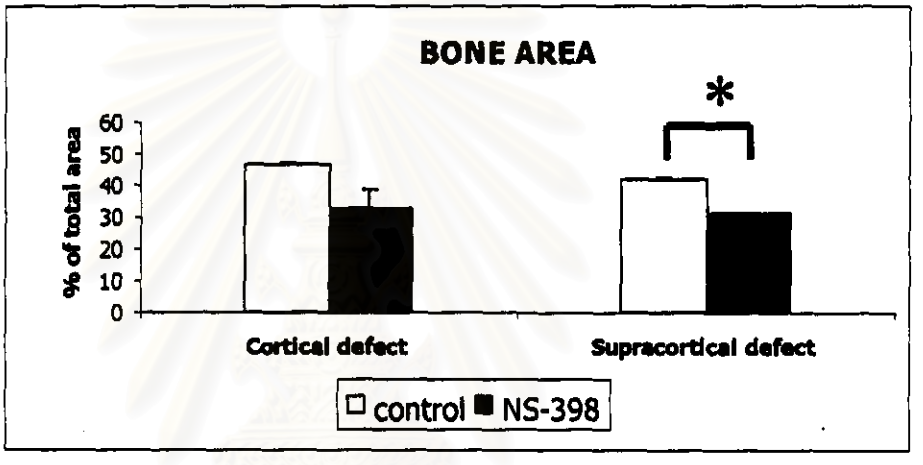

Figure 11 Effect of COX-2 inhibitor (NS-398) on bone area in cortical defect and supracortical defect. Asterisk shows a significant difference at $p < 0.05$

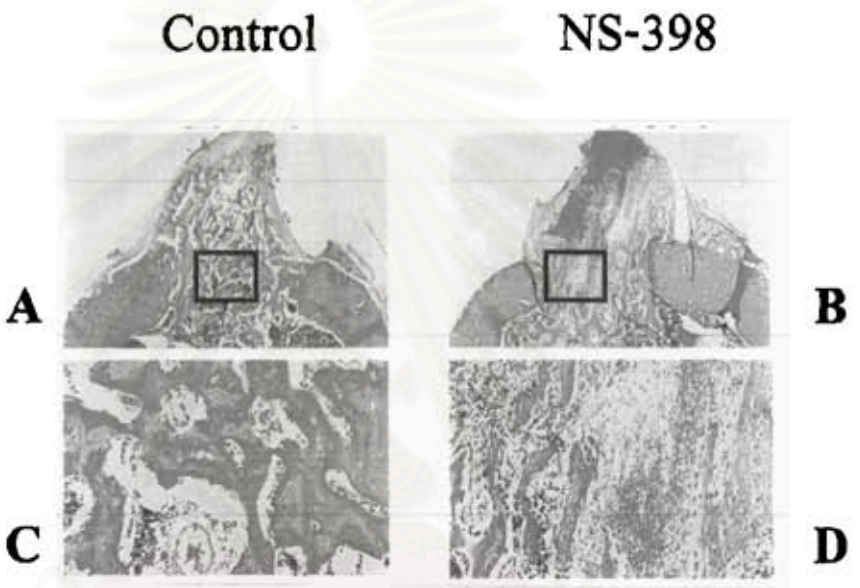

Figure 12 Effect of COX-2 inhibitor (NS-398) on bone volume in cortical defect and supracortical defect. (A and C) control, (B and D) with NS-398. H&E staining. Original magnification x40 (A and B) and x200 (C and D).

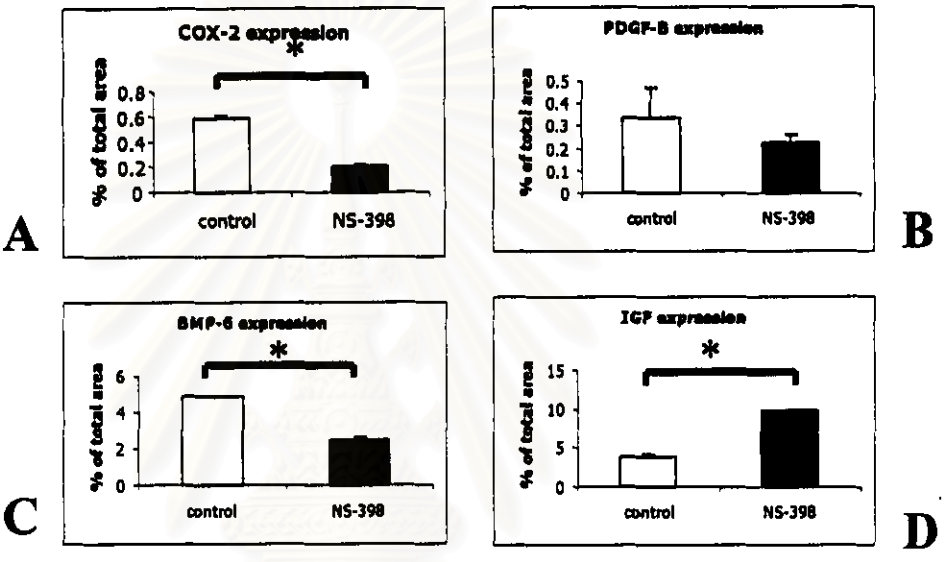

Figure 13 Effect of COX-2 inhibitor (NS-398) on the expression of COX-2 (A), PDGF-B (B), BMP-6 (C), and IGF (D) by immunological staining in cortical defect. Asterisks show a significant difference at $p < 0.05$

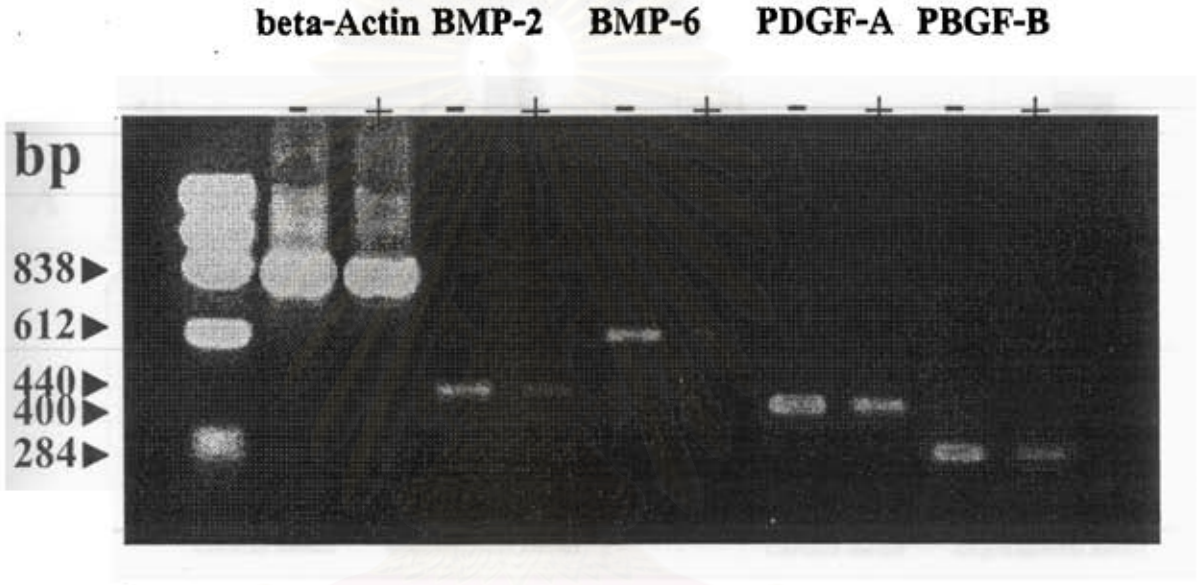

Figure 14 Detection of mRNAs for BMP-2, BMP-6, PDGF-A and PDGF-B by RT-PCR on total RNA from supracortical part of bone regeneration in control (-) and NS-398 treated (+) animal. Primers and conditions were as described in Materials and methods. An ethidium bromide stained 1.5% agarose gel is shown and the sizes for beta-Actin (838 bp), BMP-2 (440 bp), BMP-6 (612 bp), PDGF-A (400 bp) and PDGF-B (284 bp) PCR products are indicated.

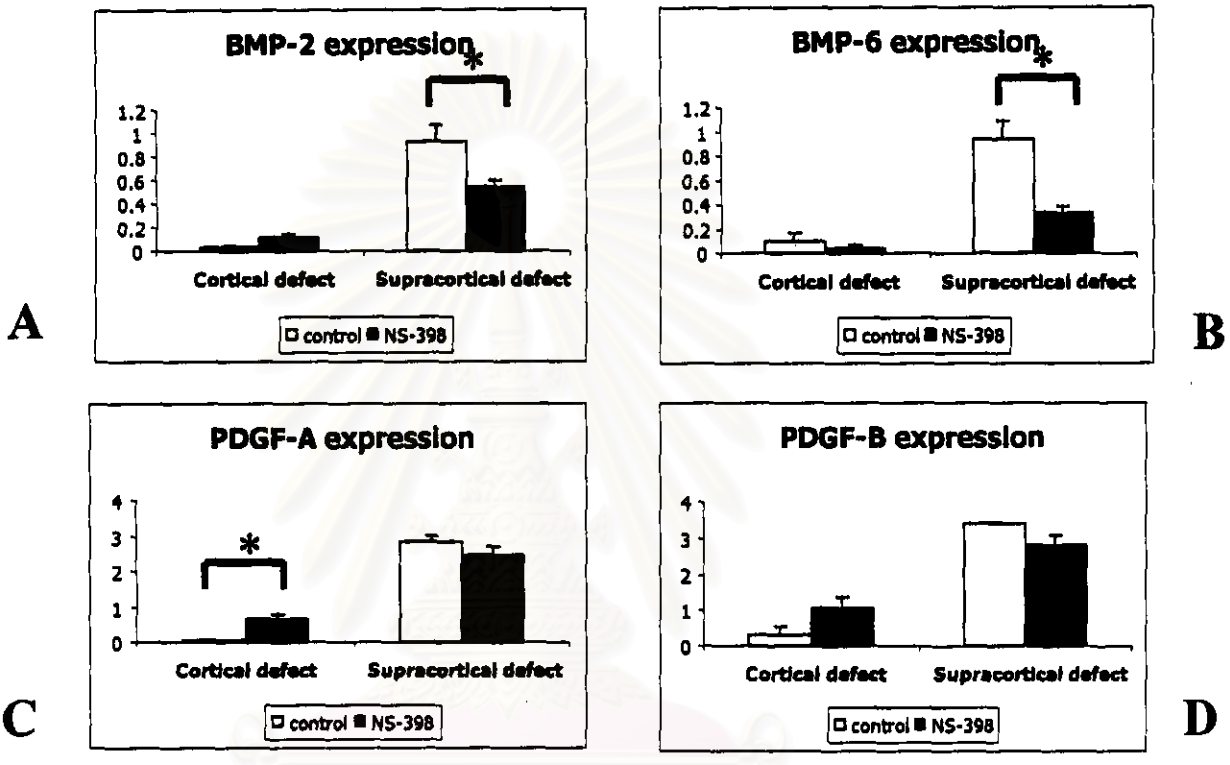

Figure 15 Effect of COX-2 inhibitor (NS-398) on the mRNA expression of BMP-2 (A), BMP-6 (B), PDGF-A (C), and PDGF-B (D). RNA was isolated from supracortical and cortical part of bone regeneration at 14 days after surgery (n= 3) and analyzed for mRNA by RT-PCR. Two to three separate samples of bone regeneration were examined and values were expressed as ratio of each growth factor mRNA level to the β-actin mRNA level. Asterisks show a significant difference at $p < 0.05$

Study III

Δ^{12}-PGJ_2 induces bone regeneration

Previous experiments in study I have established that new bone formation within the cortical defect is 40% complete by 10 days. Histological examination of control chambers confirmed this finding and revealed that the chamber space contained granulation tissue with small blood vessels. Some of the collagen sponge and a partly disintegrated blood clot were also presented at the upper part of the chamber space. The cortical defect area in all samples was partly filled with newly formed trabecular bone containing some connective tissue and bone marrow spaces. The surface of the remodeling trabecular bone showed areas of active osteoblastic bone formation as well as osteoclastic resorption. Bone formation activity can be inferred from the numerous osteoblasts observed on trabecular bone adjacent to the granulation tissue in the chamber space area and from the stain intensity. The newly formed bone trabeculae advanced from the sides of the surgically cut cortical bone as well as from the bone marrow and endosteal surfaces and were weakly stained by eosin (**Figure 16**).

Histomorphometric analysis of the cortical defect area indicated that the percentage of new bone formed increased in a dose dependent manner and 10^{-3} and 10^{-5} M of Δ^{12}-PGJ_2 induced significant increase in bone ingrowth (54% and 53% respectively) compared to those of the control (40%) (**Figure 16 and 21**). No enhancement of bone regeneration was observed at the 10^{-7} and 10^{-9} M of Δ^{12}-PGJ_2. A positive dose-response indicates that Δ^{12}-PGJ_2 is a true bone forming agonist in this model.

Figure 16 Light micrographs of new bone regeneration in the defect area 10 days after the surgery. (A) control. (B) Δ^{12}- PGJ_2 $1x10^{-7}$ M. (C) Δ^{12}-PGJ_2 $1x10^{-5}$ M. (Massons' Trichrome, original magnification x40)

Δ^{12}-PGJ_2 induces PDGF, BMP-2 and -6 expression

Cells expressing PDGF were identified in some osteoblast lining, in osteocytes in bone trabeculae and also in bone marrow space such as megakaryocytes. A significant increase of PDGF-B expression in the defect area (approximately 2.1 folds) was noticed when the 10^{-5} M dose was used (**Figure 18D and 23**), while a significant increase of both PDGF-A and -B expression (approximately 2.3 and 3.3 folds respectively) was seen when the 10^{-3} M dose was used (**Figure 17E, 18E, 22 and 23**). Osteoblasts and osteocytes were the major cell types which expressed PDGF-A and -B. Some fibroblasts in the connective tissue surrounding the bone trabeculae were found to express PDGFs as well (**Figure 17 and 18**). A significant increase of BMP-2 and BMP-6 expression in the defect area (approximately 2.8 and 2.1 folds respectively) was seen when the 10^{-3} g dose was used (**Figure 19E, 20E, 25 and 26**).

Effect of Δ^{12}-PGJ_2 on IGF expression

IGF positive staining was found in osteoblast lining cells, osteocytes and also in undifferentiated spindle shaped cells in stromal tissue and surrounding connective tissue. There was no significant increase in both area and intensity of IGF expression in cortical bone defect for any of the doses of Δ^{12}-PGJ_2 as compared to the controls (**Figure 24**).

Effect of Δ^{12} PGJ_2 on mitosis

BrdU expression in cells demonstrates that they are proliferating. Osteoblast lining cells and undifferentiated cells in the stroma were positively stained

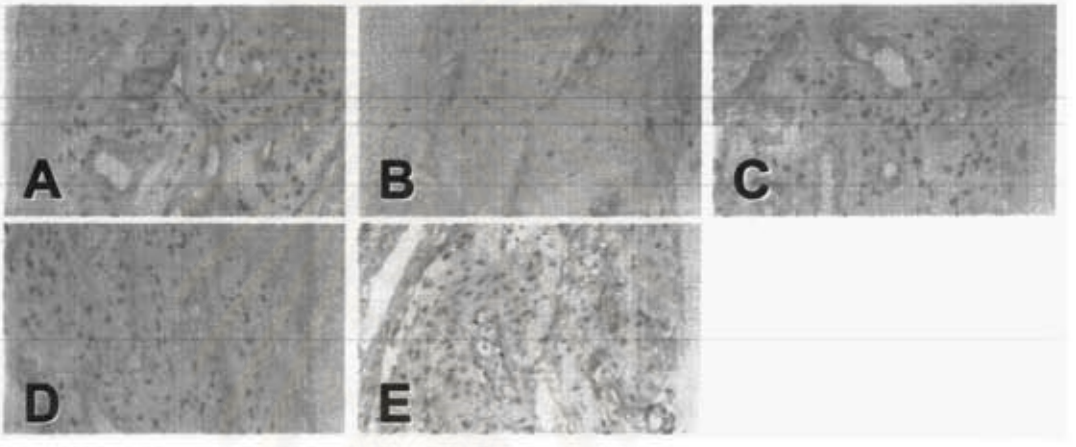

Figure 17 Light micrographs of PDGF-A expression in the defect area 10 days after the surgery. (A) control. (B) Δ^{12}-PGJ_2 $1x10^{-9}$ M. (C) Δ^{12}-PGJ_2 $1x10^{-7}$ M. (D) Δ^{12}-PGJ_2 $1x10^{-5}$ M. (E) Δ^{12}-PGJ_2 $1x10^{-3}$ M. (original magnification x200)

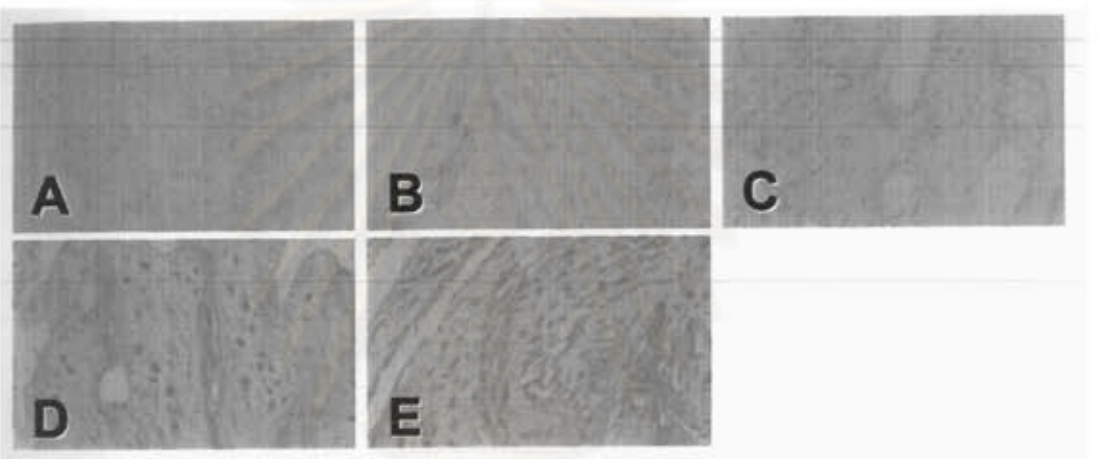

Figure 18 Light micrographs of PDGF-B expression in the defect area 10 days after the surgery. (A) control. (B) Δ^{12}-PGJ_2 $1x10^{-9}$ M. (C) Δ^{12}-PGJ_2 $1x10^{-7}$ M. (D) Δ^{12}-PGJ_2 $1x10^{-5}$ M. (E) Δ^{12}-PGJ_2 $1x10^{-3}$ M. (original magnification x200)

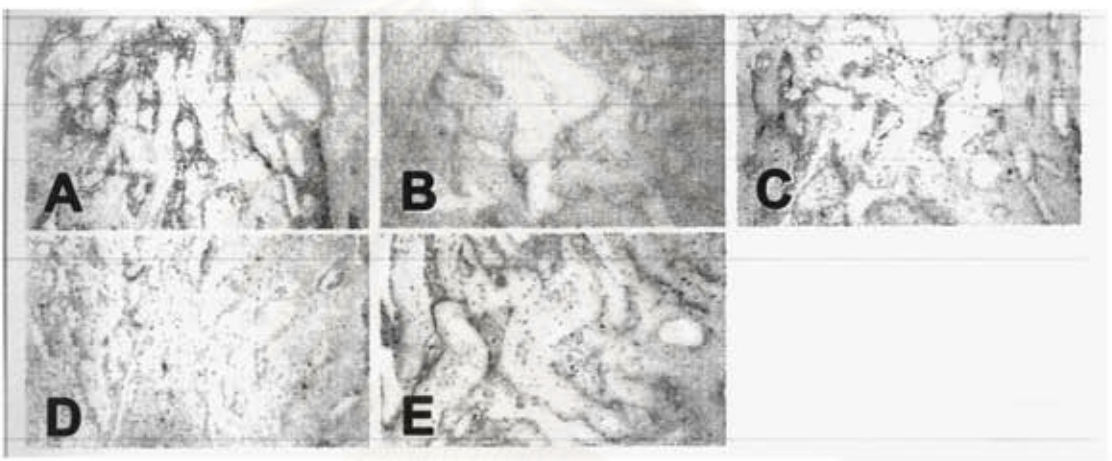

Figure 19 Light micrographs of BMP-2 expression in the defect area 10 days after the surgery. (A) control. (B) Δ^{12}-PGJ_2 $1x10^{-9}$ M. (C) Δ^{12}-PGJ_2 $1x10^{-7}$ M. (D) Δ^{12}-PGJ_2 $1x10^{-5}$ M. (E) Δ^{12}-PGJ_2 $1x10^{-3}$ M. (original magnification x200)

Figure 20 Light micrographs of BMP-6 expression in the defect area 10 days after the surgery. (A) control. (B) Δ^{12}-PGJ_2 $1x10^{-9}$ M. (C) Δ^{12}-PGJ_2 $1x10^{-7}$ M. (D) Δ^{12}-PGJ_2 $1x10^{-5}$ M. (E) Δ^{12}-PGJ_2 $1x10^{-3}$ M. (original magnification x200)

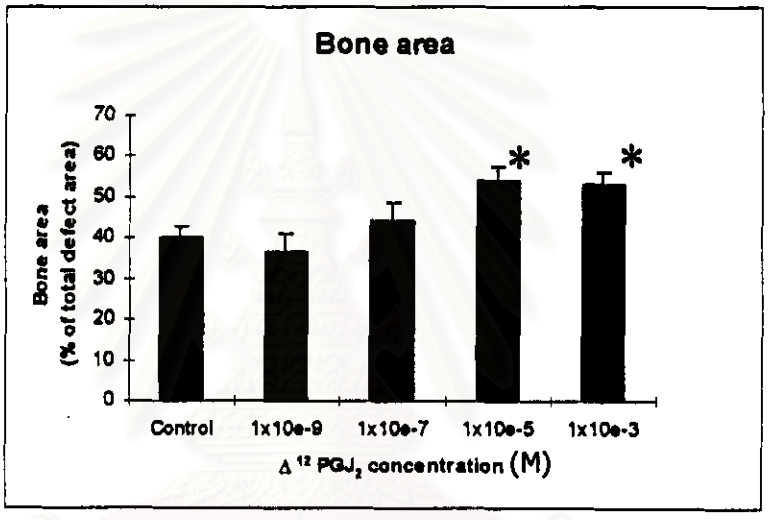

Figure 21 Effect of Δ^{12}-PGJ_2 on new bone regeneration. Data are expressed as the mean ± SEM. Asterisks show a significant difference from control value at $p < 0.05$.

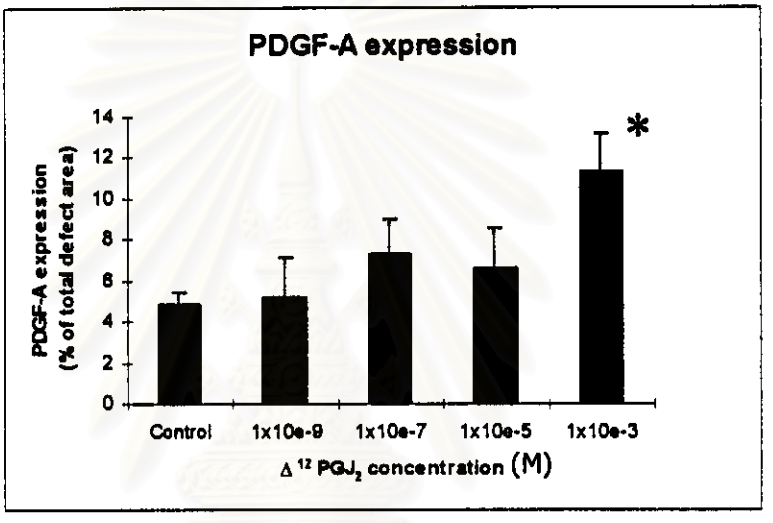

Figure 22 Effect of Δ^{12}-PGJ_2 on PDGF-A expression. Data are expressed as the mean $\pm$ SEM. Asterisk shows a significant difference from control value at $p < 0.05$.

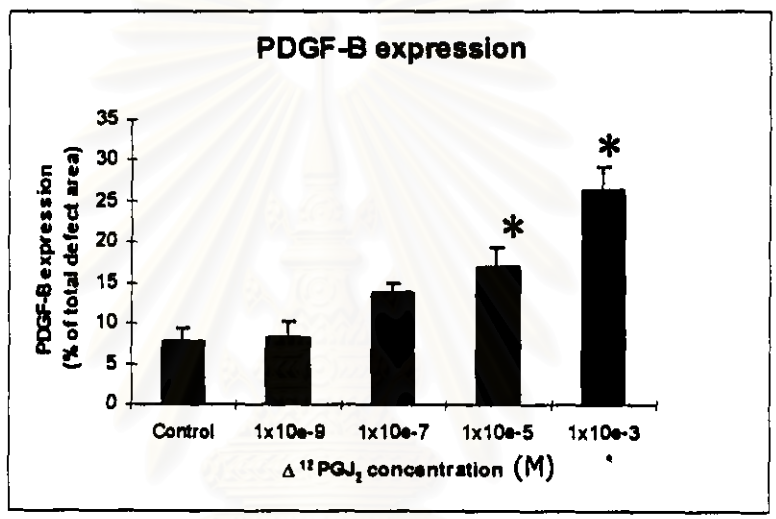

Figure 23 Effect of Δ^{12}-PGJ_2 on PDGF-B expression. Data are expressed as the mean $\pm$ SEM. Asterisks show a significant difference from control value at $p < 0.05$.

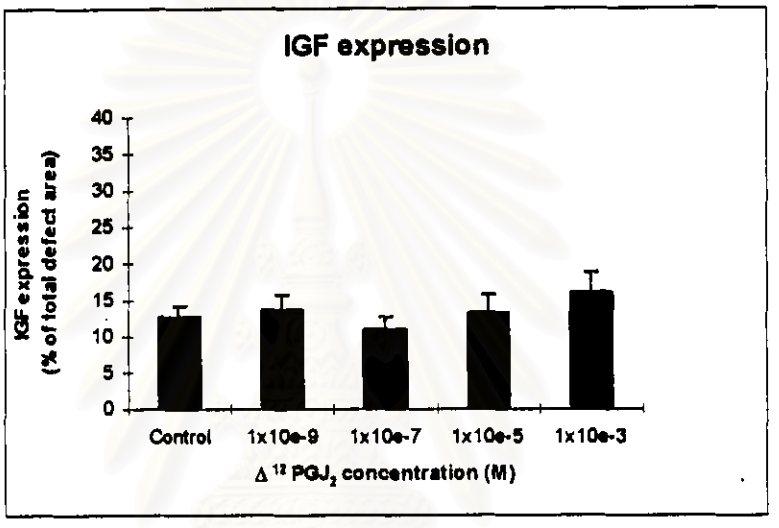

Figure 24 Effect of Δ^{12}-PGJ_2 on IGF expression. Data are expressed as the mean $\pm$ SEM.

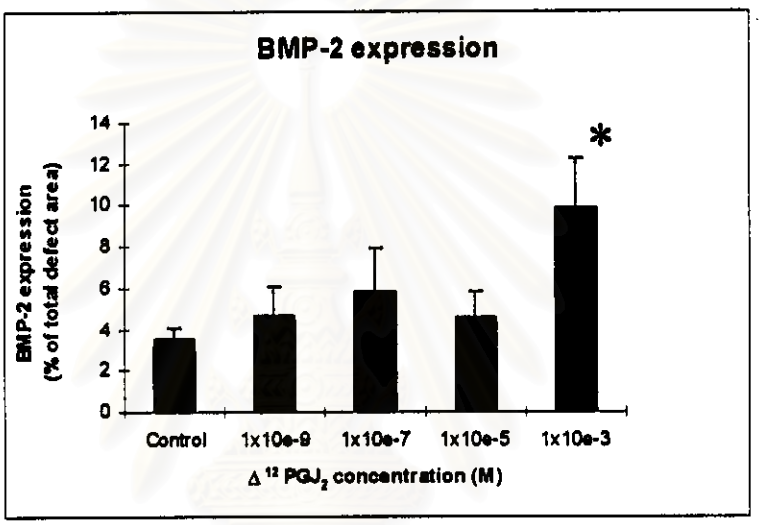

Figure 25 Effect of Δ^{12}-PGJ_2 on BMP-2 expression. Data are expressed as the mean $\pm$ SEM. Asterisk shows a significant difference from control value at $p < 0.05$.

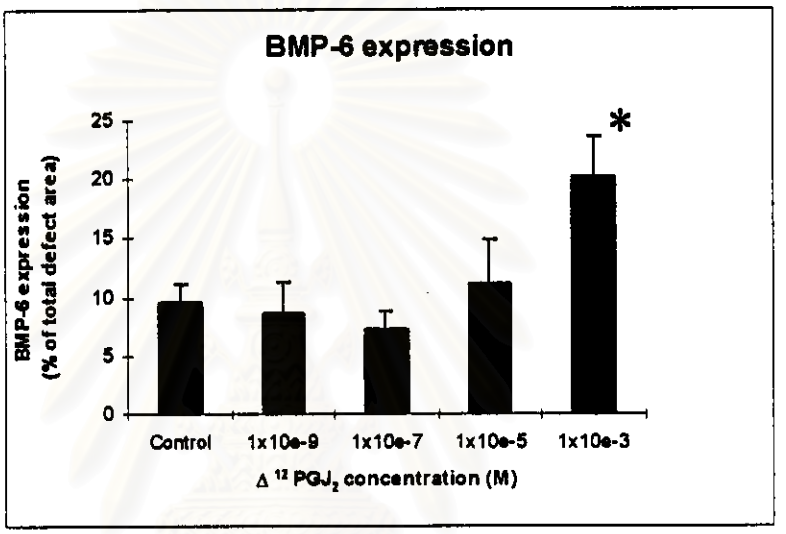

Figure 26 Effect of Δ^{12}-PGJ_2 on BMP-6 expression. Data are expressed as the mean $\pm$ SEM. Asterisk shows a significant difference from control value at $p < 0.05$.

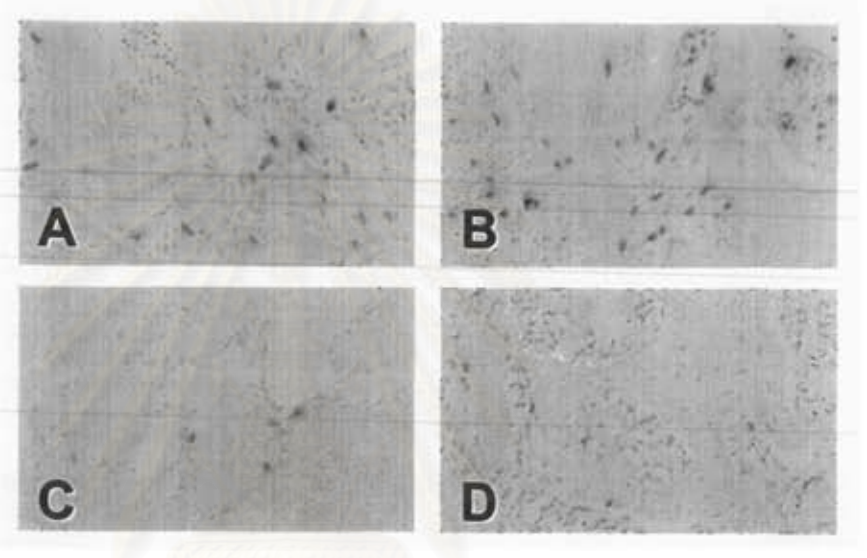

Figure 27 Light micrographs of BrdU-positive cells in the defect area 10 days after the surgery. Sections were exposed to a monoclonal anti-BrdU antibody, and revealed with a highly sensitive streptavidin-biotin staining system. (DAB) mixed with hydrogen peroxide was used as a chromogen, staining BrdU-incorporated nuclei a dark brown color. (A) control. (B) Δ^{12}-PGJ_2 $1x10^{-7}$ M. (C) Δ^{12}-PGJ_2 $1x10^{-5}$ M. (D) Δ^{12}-PGJ_2 $1x10^{-3}$ M. (original magnification x200)

for BrdU. The 10^{-7} M dose of Δ^{12}-PGJ_2 led to an increase in the number of positive cells in the defect area (51 ± 12) but no statistical significance was noticed as compared to the control (36 ± 9) and the 10^{-3} M dose (29 ± 3) (**Figure 27**).

Study IV

Δ^{12}-PGJ_2 induces new bone regeneration surrounding titanium implant

All the implants were found to be stable in the bone at the time of sacrifice. Macroscopically, there was no obvious adverse tissue reaction. The central section that is made through the center axis of the implant was used in this study to avoid the shadow effect error from the circular curve of the round surface of the screw-shaped implant (Johansson and Morberg, 1995). The proper thickness of the sections is also important for quantification in order to achieve reliable results. The 100 μm thickness sections were used in this study since the bone area in the threads appeared to be similar irrespective of section thickness from 10 to 100 μm (Johansson and Morberg, 1995). The implants were located in two parts of the femoral bone: transcortical portion and trabecular / marrow compartment (**Figure 28**). Mostly, the first one or two threads of the implants were in the transcortical part. The major part of new bone formed around the implants was the new bone regeneration from the endosteal surface enclosing the implants. New bone regeneration around the implants in subendosteal area was analyzed. Data from animals which were treated with $1x10^{-5}$ and $1x10^{-3}$ M Δ^{12}-PGJ_2 were pooled together since there was no significant difference between those two concentrations. Δ^{12}-PGJ_2 significantly increased new bone regeneration around the implants at endosteal surface of the cortical bone by increasing both vertical distance and thickness of new bone regeneration (34% and 59% respectively) at 8

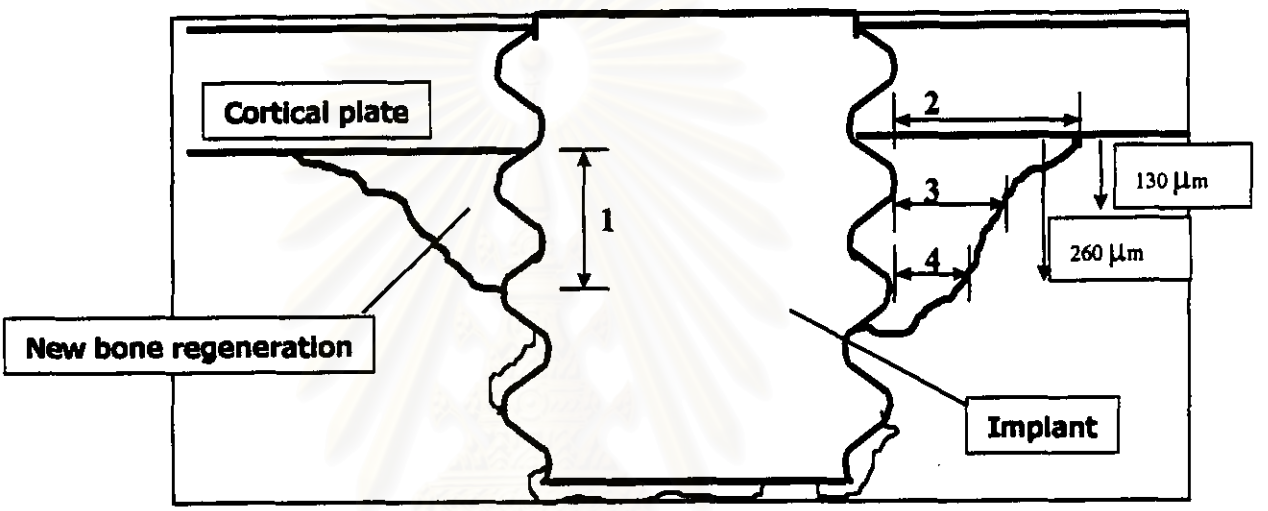

Figure 28 Schematic presentation of histomorphometry analysis of new bone regeneration around titanium implant. (1), vertical distance of new bone regeneration from endosteal surface to the most apical point. (2), (3), (4), horizontal distance of new bone regeneration from implant surface at endosteal surface, 130 µm and 260 µm below endosteal surface respectively.

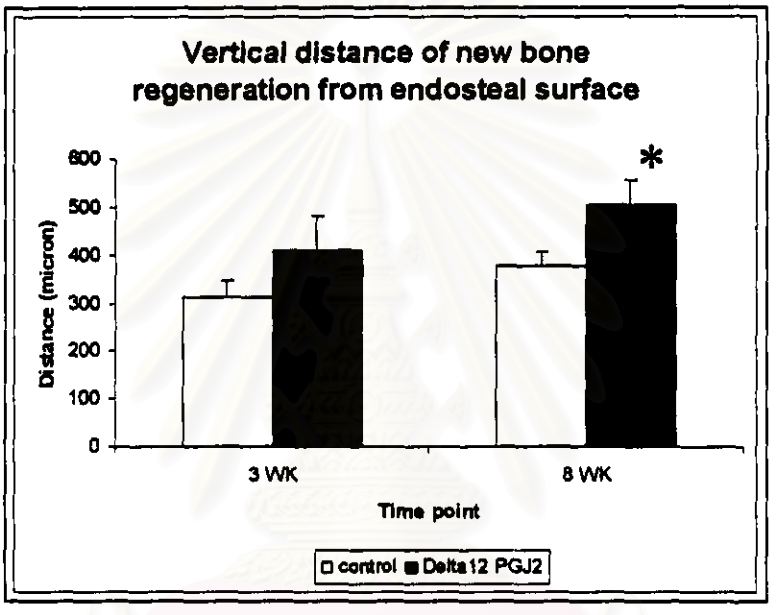

Figure 29 Effect of Δ^{12}-PGJ_2 on vertical distance of new bone regeneration at 3 weeks and 8 weeks. Data are expressed as the mean $\pm$ SEM. Asterisks show a significant difference from control value at $p < 0.05$.

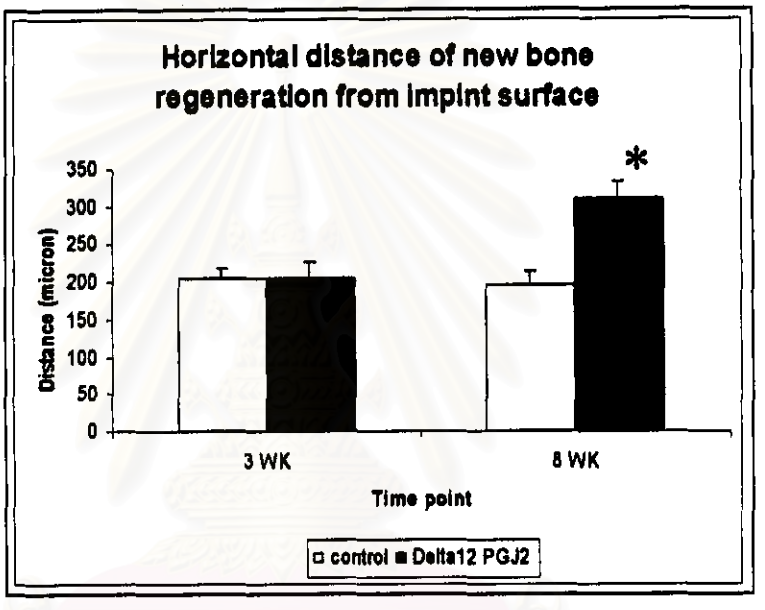

Figure 30 Effect of Δ^{12}-PGJ_2 on horizontal distance of new bone regeneration at 3 weeks and 8 weeks. Data are expressed as the mean $\pm$ SEM. Asterisks show a significant difference from control value at $p < 0.05$.

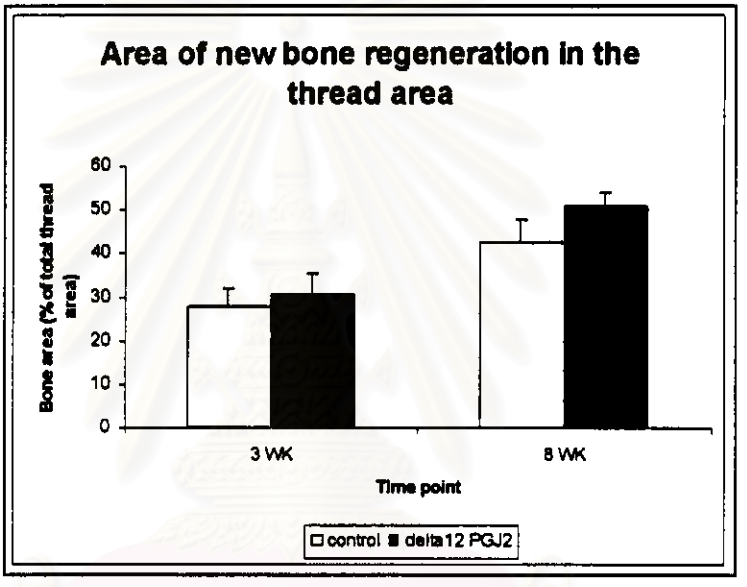

Figure 31 Effect of Δ^{12}-PGJ_2 on new bone regeneration in thread area at 3 weeks and 8 weeks. Data are expressed as the mean $\pm$ SEM.

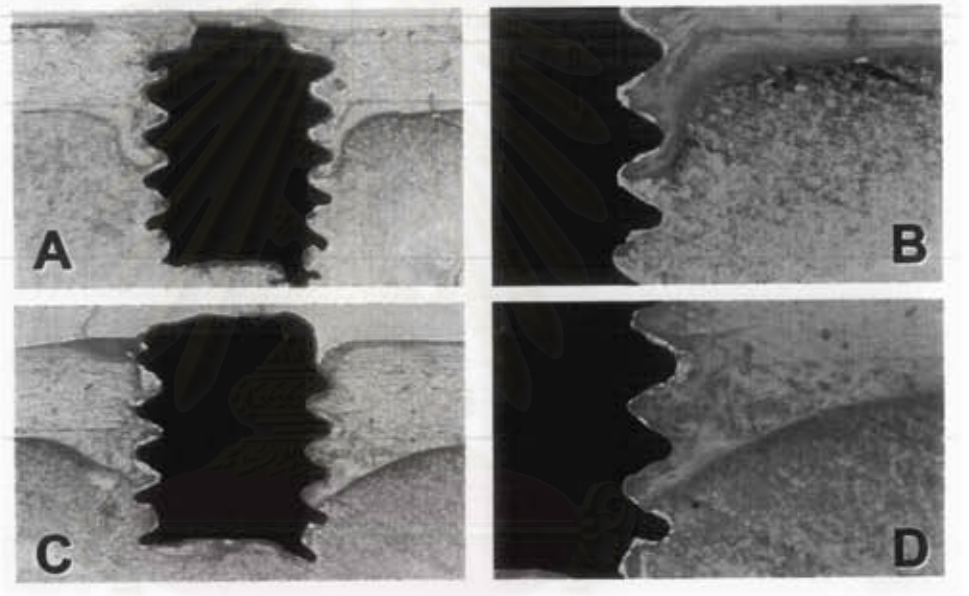

Figure 32 New bone regeneration around titanium implant at 8 weeks after surgery. (A) and (B) control; (C) and (D) Δ^{12}-PGJ_2 (toluidine blue staining, original magnification x20 (A and C), original magnification x40 (B and D).

weeks (**Figure 29, 30 and 32**) but not significant difference at 3 weeks. There is no significant difference in bone regeneration area in the thread between control and Δ^{12}-PGJ_2 even though increasing tendency were observed in both 3 and 8 weeks (**Figure 31**).